

## Letters

### Discovery of a Series of 6,7-Dimethoxy-4-pyrrolidylquinazoline PDE10A Inhibitors<sup>†</sup>

Thomas A. Chappie,\* John M. Humphrey, Martin P. Allen, Kimberly G. Estep, Carol B. Fox, Lorraine A. Lebel, Spiros Liras, Eric S. Marr, Frank S. Menniti, Jayvardhan Pandit, Christopher J. Schmidt, Meihua Tu, Robert D. Williams, and Feng V. Yang

CNS Discovery and Experimental Medicinal Sciences, Pfizer Global Research and Development, Eastern Point Road, Groton, Connecticut 06340

Received June 1, 2006

**Abstract:** A papaverine based pharmacophore model for PDE10A inhibition was generated via SBDD and used to design a library of 4-amino-6,7-dimethoxyquinazolines. From this library emerged an aryl ether pyrrolidyl 6,7-dimethoxyquinazoline series that became the focal point for additional modeling, X-ray, and synthetic efforts toward increasing PDE10A inhibitory potency and selectivity versus PDE3A/B. These efforts culminated in the discovery of **29**, a potent and selective brain penetrable inhibitor of PDE10A.

The phosphodiesterases (PDEs) are a family of widely expressed enzymes that hydrolyze the 3′–5′ phosphodiester bond of the ubiquitous intracellular messenger molecules cyclic adenosine monophosphate (cAMP) and cyclic guanosine monophosphate (cGMP) to effect signal termination. The PDEs are encoded by 21 different genes in humans, with over 60 isoforms expressed as a result of alternative splicing patterns.<sup>1</sup> Although considerable variation is possible among the full-length enzymes, the catalytic domains share common functionality and similar modular structures with several conserved amino acid residues. Key residues in the catalytic core form a hydrophobic pocket that accommodates the planar nucleotide in a spatial orientation that facilitates hydrogen bonding to an absolutely conserved glutamine residue.<sup>2</sup> Variations in the amino acid sequence at the catalytic domain and elsewhere give rise to unique substrate specificities, catalytic efficiencies, and pharmacologies and permit subdivision of the PDEs into 11 distinct families. Given the unique role of each PDE in regulating cyclic nucleotide signaling in various organ systems, it is not surprising that research in this area has produced marketed drugs for a variety of disease states.<sup>3–7</sup> Critical to the continued success of such efforts is the ability to identify and exploit the subtle structural differences within the catalytic cores of the different PDE isoforms.

PDE10A is the single member of a dual substrate (cGMP/cAMP) family first reported in 1999.<sup>8–11</sup> The enzyme is heavily expressed by the medium spiny neurons of the mammalian striatal complex,<sup>12,13</sup> making it an intriguing target for the treatment of diseases of the central nervous system. Work from our laboratories shows that papaverine, a naturally occurring plant alkaloid and smooth muscle relaxant, is a relatively potent inhibitor of PDE10A, exhibiting moderate cross-reactivity versus

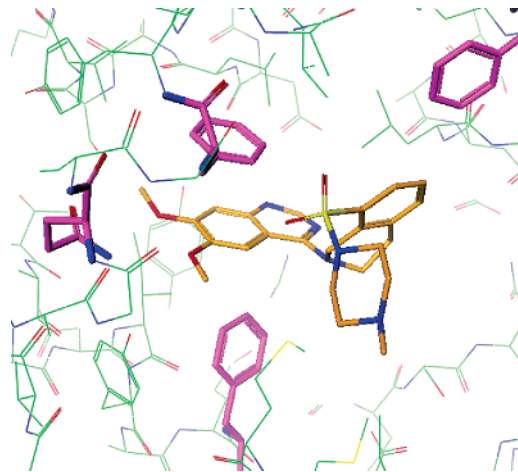


**Figure 1.** Cocystal structure of **1** bound to the PDE10A catalytic site. Important PDE10A binding residues are highlighted in magenta.

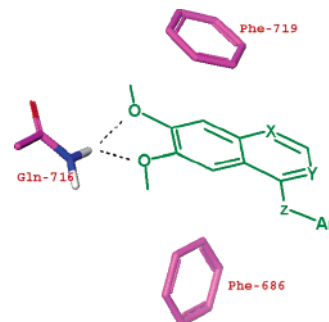


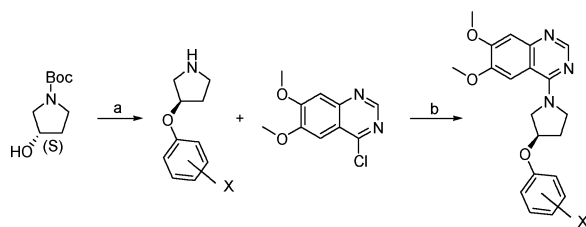
**Figure 2.** PDE10A schematic pharmacophore model.

PDE3A and 3B ( $K_i = 17, 279,$  and  $417$  nM, respectively). In studies employing papaverine as a pharmacological probe in wild type and PDE10A knock out mice, we have found evidence to suggest that PDE10A inhibitors may be effective for the treatment of psychosis in schizophrenia.<sup>14–16</sup> To advance this theory, we initiated a chemistry effort aimed at designing more potent and selective pharmacological tools to further our understanding of PDE10A physiology and the therapeutic potential of PDE10A inhibitors. This search for a new class of PDE10 inhibitors was based on the structure of papaverine.

The recently reported tetrahydroquinolinyl dimethoxyquinazoline derivative (**1**, Figure 1),<sup>17</sup> derived from a file screen hit, was an attractive starting point for these studies due to its reasonable potency versus PDE10A ( $K_i = 25$  nM) and structural similarity to papaverine. In addition, chemical design would be greatly facilitated by access to the X-ray crystal structure of compound **1** bound within the catalytic subunit of PDE10A.<sup>18</sup> According to this structure, the inhibitor **1** forms two key interactions. In the first of these, a bidentate hydrogen-bonding interaction between Gln-716 and the two methoxy groups of the quinazoline ring, in which the methoxy groups share a single N–H proton donated by the glutamine residue, anchors the ligand within the active site. In the second essential interaction the planar quinazoline ring occupies a hydrophobic region defined by the residues Phe-719 and Phe-686 (Figure 2). In doing so, the quinazoline achieves a  $\pi$ -stacking interaction with

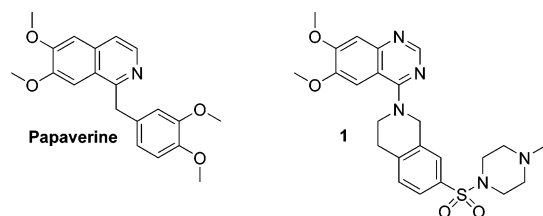
<sup>†</sup> PDB ID code: 208H.

\* To whom correspondence should be addressed. Phone: (860) 715-5142. Fax: (860) 686-1059. E-mail: thomas.a.chappie@pfizer.com.

Scheme 1. Synthesis of **8–29**<sup>a</sup>

<sup>a</sup> Reagents and conditions: (a) (i) ArOH, DEAD, PPh<sub>3</sub>, THF, rt, 16 h; (ii) TFA, CH<sub>2</sub>Cl<sub>2</sub>, rt, 4 h, 66–99%; (b) 4-chloro-6,7-dimethoxyquinazoline, K<sub>2</sub>CO<sub>3</sub>, PhCH<sub>3</sub>, 80 °C, 16 h, 45–99%.

the “upper” residue, Phe-719, and an edge-on interaction with Phe-686 located at the bottom of the pocket. Additional favorable hydrophobic binding interactions occur between the aryl portion of the tetrahydroisoquinoline fragment of **1** and the protein, while the sulfonamide group is exposed to solvent.



Information obtained from the X-ray structure of bound **1** and from modeling studies with papaverine enabled construction of a schematic PDE10A “pharmacophore model” that we would use to design new compounds (Figure 2). The model is comprised of three parts. First, a dimethoxy component is employed to retain the bidentate Gln-716 hydrogen bond interaction observed in **1**. Second, a fused biaryl ring system attached to the dimethoxy component occupies the hydrophobic clamp defined by Phe-719 and Phe-686. Last, an aryl group is appropriately attached to mimic the substituent aryl rings of papaverine and **1**, thereby increasing affinity through nonspecific hydrophobic interactions with the protein (Figure 2).

Using this information, new inhibitor design efforts began in parallel to work on **1**. In advance of the chemical synthesis, we prepared a virtual library of >2000 6,7-dimethoxyquinazolines substituted at C4 with various aryl-bearing amine components. The library was filtered by calculated properties predictive of good ADME, including molecular weight, cLogP, and TPSA, to afford some 300 compounds for actual library synthesis. The synthetic work simply required coupling of 4-chloro-6,7-dimethoxyquinazoline<sup>19–21</sup> with the filtered set of aryl-bearing amines identified from the virtual library (Scheme 1, step b). HPLC purification afforded the desired products in moderate yield. Upon analysis of the products, a collection of chiral 4-pyrrolidyl-6,7-dimethoxyquinazolines emerged as promising leads due to moderate PDE10A potency and discernible SAR (compounds **2–8**, Table 1). Although potency and selectivity were compromised in relation to **1**, the series provided many advantages with respect to physical chemical properties needed for a CNS-based target. Also evident from this library was that (i) the greatest PDE10A inhibitory activity resided with the R-isomer; (ii) PDE3A and PDE3B inhibitory activity was present and considerable, and (iii) as indicated by compound **8**, achievement of PDE10A selectivity over PDE3A/B appeared possible.

Comparable potency and selectivity observed with **8** versus papaverine warranted development of an efficient enantioselective synthesis of this chemotype. Thus, a small set of new

Table 1. PDE K<sub>i</sub><sup>a</sup>

#	X =	PDE10A	PDE3A	PDE3B
<b>2</b>	2-CF <sub>3</sub>	811	<100	>100
<b>3</b>	2-CH <sub>3</sub>	326	<100	<100
<b>4</b>	2-OCH <sub>3</sub>	240	<100	>100
<b>5</b>	2-OCH <sub>3</sub> (S)-ent	641	>100	>100
<b>6</b>	2-Cl	198	<100	<100
<b>7</b>	2-CN	130	<100	<100
<b>8</b>	4-CN	56	214 (4×)	471 (8×)
<b>9</b>	4-OCF <sub>3</sub>	185	739 (4×)	1820 (10×)
<b>10</b>	4- <i>t</i> -Bu	100	720 (7×)	1890 (19×)
<b>11</b>	4-OEt	54	161 (3×)	328 (6×)

<sup>a</sup> Reported in nM. Selectivity vs PDE3A/B in parenthesis.

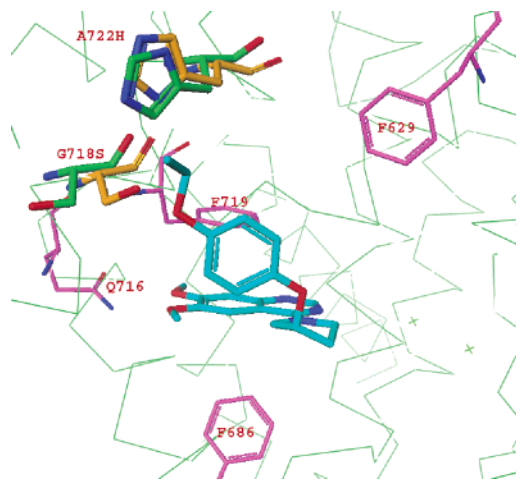


Figure 3. Cocystal structure of **11** (cyan) bound to the PDE10A catalytic site. Important residues are highlighted in PDE10A (magenta) and PDE3A/B (yellow/green).

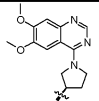
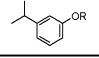
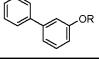
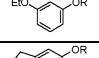
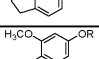
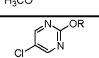
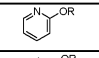
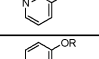
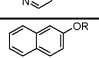
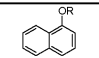
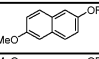
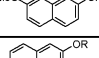
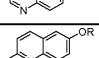
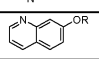
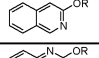
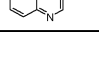
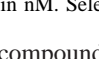
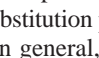
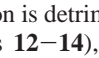
analogues were prepared manually beginning with commercial *N*-*t*-Boc-(*S*)-3-hydroxyproline. Inversion at C3 and concurrent substitution with variously substituted phenols was accomplished via the Mitsunobu reaction and provided, after deprotection, the 3-aryloxy pyrrolidines in acceptable yield.<sup>22</sup> Reaction with 4-chloro-6,7-dimethoxyquinazoline proceeded efficiently, providing the *para*-substituted target compounds **8–11** (Scheme 1).

At this point, X-ray diffraction studies and computational modeling assumed a prominent role in our efforts to understand PDE10/PDE3 selectivity. Paramount to these efforts was our structure elucidation of the complex formed between the catalytic domain of PDE10A and ligand **11**. Coordinates from these studies were overlaid with those provided by an in-house homology model of the catalytic domains of PDE3A/B to highlight regional differences between the enzymes and to generate ideas for designing selective compounds (Figure 3).

Overlay of PDE3A/B homology model with PDE10 X-ray structure reveals that a synthetically accessible difference exists in the region proximal to the aryl ether appendage of bound ligand. Specifically, the small residues Gly-718 and Ala-722 of PDE10 are replaced by the larger amino acids Ser (G718S) and His (A722H), respectively, in both PDE3A and PDE3B. Steric hindrance thus appeared to play a determinant role in the observed PDE3B selectivity gains with ligand **11** versus less selective ligands. The observation that analogs possessing *para*-substitution patterns on the aryloxy ring achieved greater selectivity and potency than *ortho*-substituted analogs guided us in our next design efforts, which are shown in Table 2.

A diverse set of 3-aryloxy and 3-heteroaryloxy pyrrolidine analogs were synthesized according to the route of Scheme 1.

Table 2. PDE  $K_i^a$ 

#		PDE10A	PDE3A	PDE3B
12		171	370 (2 x)	474 (3 x)
13		136	271 (2 x)	280 (2 x)
14		94	61 (<1 x)	88 (1 x)
15		68	141 (2 x)	237 (3.5 x)
16		67	121 (2 x)	260 (4x)
17		44	162 (4 x)	332 (7.5 x)
18		123	77 (<1x)	207 (2 x)
19		128	302 (2 x)	748 (6 x)
20		112	226 (2 x)	685 (6x)
21		12	283 (24 x)	463 (39 x)
22		210	48 (<1x)	56 (<1 x)
23		18	199 (11 x)	280 (16x)
24		17	273 (16 x)	305 (18 x)
25		12	104 (9 x)	201 (17 x)
26		18	152 (8 x)	223 (12 x)
27		12	209 (17x)	240 (20 x)
28		19	151 (8x)	196 (10x)
29		4	211 (53x)	273 (68x)

<sup>a</sup> Reported in nM. Selectivity vs PDE3A/B in parenthesis.

These new compounds were designed to assess the effects of other aryl substitution patterns and pyridyl ring systems on PDE inhibition. In general, the data indicates that steric bulk in the *meta*-position is detrimental to activity versus all three enzymes (compounds **12**–**14**), whereas relatively smaller groups in a *meta*-/*para*-disubstitution pattern provided no improvements in PDE10 potency and selectivity (**15** and **16**). 5-Cloropyrimidine **17** provides potency equivalent to papaverine but without significant selectivity.

Gains in both potency and selectivity were finally realized in a subset of these compounds (**21**–**29**) wherein the simple monocyclic aryl ethers were replaced with larger aromatic- and heteroaromatic-bicyclic ethers. As evident from a comparison of **21** and **22**, the 2-naphthyl group offers far greater PDE10 potency over the 1-naphthyl group ( $K_i = 12$  nM vs 210 nM, respectively) and improved selectivity over PDE3A/B. Methoxy substitution did not enhance the selectivity (**21** vs **23** and **24**). Various other quinoline and isoquinoline ring systems were examined in anticipation of improved PDE10 potency as was observed with the pyrimidine **17**. For the most part, however, these analogs exhibited PDE10 potencies comparable with **21** and reduced selectivities spanning a range from  $\sim 8\times$  to  $\sim 20\times$ . In a particularly favorable discovery, (*R*)-6,7-dimethoxy-4-(3-(quinoxalin-2-yl)oxy)pyrrolidin-1-yl)quinazoline **29** proved to be the most potent (4 nM) and selective (53–68-fold) PDE10 inhibitor of this quinazolinone campaign and, furthermore, exhib-

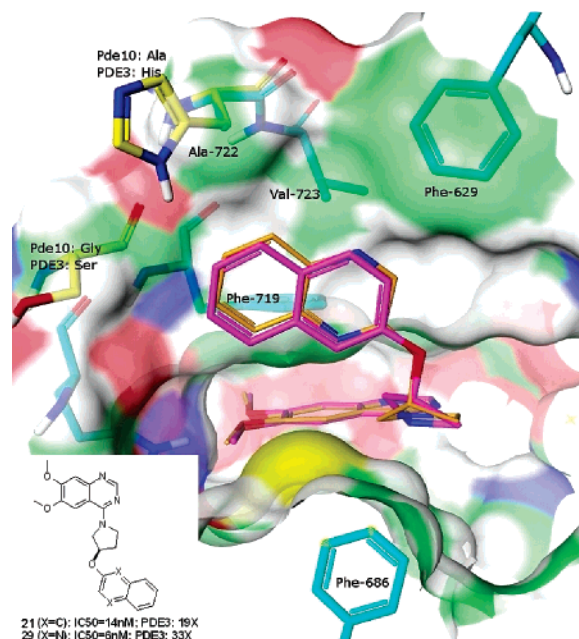


**Figure 4.** Overlaid crystal structures of **21** (magenta) and **29** (orange) in PDE10A. PDE3A/B residues yielding unfavorable steric interactions are included as overlays.

ited  $>38$ -fold selectivity for PDE10 when assessed versus a panel of 60 different CNS-associated receptors, enzymes, and ion channels.

X-ray structures of PDE10A–inhibitor complexes with compounds **21** and **29** reveal nearly identical binding modes for each (Figure 4). Evident from these images is that increased potency of this subset, relative to the mono-aryl derivatives, is likely due to enhanced lipophilic interactions between the naphthyl/quinoxaline ring and underlying hydrophobic residues (Ala-722, Val-723, Phe-719) of the enzyme. Also overlaid on the PDE10 structure in Figure 4 are the two PDE3A/B residues, Ser and His, to which we attribute reduced PDE3 affinity. For the sake of clarity, we have shown rotamers of these residues that are turned away from the bound ligand; however, it is understood that free rotation of the His and Ser sidechains would serve to reduce the effective size of the PDE3 binding pocket relative to PDE10.

In light of its attractive *in vitro* properties, **29** was further investigated for evidence of the ability to inhibit PDE10A *in vivo*. In previous studies we noted that administration of papaverine to mice causes a rapid elevation in levels of cGMP and a concomitant increase in the phosphorylation of the downstream transcription factor cAMP response element binding protein (CREB) in the striatal regions of the brain.<sup>14</sup> These effects are consistent with the high level of expression of PDE10A in this brain region<sup>13</sup> and the ability of PDE10A to metabolize both cGMP and cAMP.<sup>8–11</sup> That the effect of papaverine is due specifically to inhibition of PDE10A is confirmed by the finding that papaverine has no effect in mice in which the gene for PDE10A has been disrupted (i.e., PDE10A knockout mice).<sup>15</sup> Thus, we investigated the effects of **29** on striatal cGMP and CREB phosphorylation in mice.

Compound **29** administered subcutaneously (32 mg/kg) caused a dose-dependent increase in striatal cGMP level after 30 min (Supporting Information). This effect of **29** was evident for at least 90 min after administration and was completely attenuated at 240 min after administration (Figure 5). Compound **29** also caused an increase in striatal CREB phosphorylation over a time course similar to that for the elevation of striatal



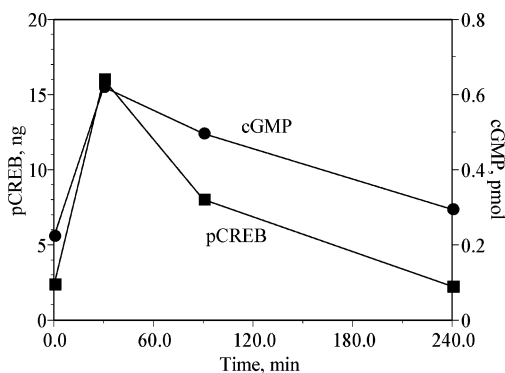


**Figure 5.** The time course of effect of **29** (32 mg/kg, s.c. in 40%  $\beta$ -cyclodextrin) on striatal cGMP and phosphorylated CREB levels in mice.

cGMP (Figure 5). These results indicate that **29** inhibits PDE10A in the brain after systemic administration. Compound **29** is somewhat more potent than papaverine on a mg/kg basis. Notably, the duration of action of **29** is considerably longer than that of papaverine, comparing present results with those reported in Siuciak et al.<sup>14</sup> Thus, given the favorable *in vitro* potency and selectivity and *in vivo* activity profile, **29** represents an important new pharmacological tool to investigate the physiology and therapeutic utility of PDE10A.

In summary, X-ray data from the ligand 1/PDE10A catalytic site complex provided a schematic pharmacophore model that was used to guide efforts toward a new series of inhibitors illustrated by **11**. With further X-ray data and computational modeling, differences in the PDE10A and PDE3A/B catalytic sites were identified and exploited to give compounds with enhanced PDE10A potency and selectivity. The culmination of this work led to **29**, a potent (4 nM) and selective (>38-fold vs PDEs and CNS related targets) compound that increases cGMP and pCREB levels in mouse striatum in a dose- and time-dependent manner. Compound **29** is currently being used as a tool to further elucidate PDE10A inhibitory activity on brain function.

**Acknowledgment.** We thank S. Simons, K. Fennel, and T. Subashi for cloning and expression of the recombinant protein construct used in the crystallography experiments.

**Supporting Information Available:** Combinatorial experimental conditions, experimental crystal structure data, computational models, and chemical and biological experimental details. This material is available free of charge via the Internet at <http://pubs.acs.org>.

## References

- Manallack, D. T.; Hughes, R. A.; Thompson, P. E. The Next Generation of Phosphodiesterase Inhibitors: Structural Clues to Ligand and Substrate Selectivity of Phosphodiesterases. *J. Med. Chem.* **2005**, *48* (10), 3449–3462.
- Card, G. L.; England, B. P.; Suzuki, Y.; Fong, D.; Powell, B.; Lee, B.; Luu, C.; Tabrizizad, M.; Gillete, S.; Ibrahim, P. N.; Artis, D. R.; Bollag, G.; Milburn, M. V.; Kim, S.; Schlessinger, J.; Zang, K. Y. J. Structural Basis for the Activity of Drugs that Inhibit Phosphodiesterases. *Structure* **2004**, *12*, 2233–2247.
- Setter, S. M.; Iltz, J. L.; Fincham, J. E.; Campbell, R. K.; Baker, D. E. Phosphodiesterase 5 Inhibitors for Erectile Dysfunction. *Ann. Pharmacol.* **2005**, *39* (7/8), 1286–1295.
- Young, R. A.; Ward, A. Milrinone. A Preliminary Review of its Pharmacological Properties and Therapeutic Use. *Drugs* **1988**, *36* (2), 158–192.
- Liu, Y.; Shakur, Y.; Yoshitake, M.; Kambayashi, J.-L. Cilostazol (Pletal): A Dual Inhibitor of Cyclic Nucleotide Phosphodiesterase Type 3 and Adenosine Uptake. *Cardiovasc. Drug Rev.* **2001**, *19* (4), 369–386.
- Wang, P.; Billah, M. M. Phosphodiesterase-4 (PDE4) as a Target for Anti-Inflammatory Drug Discovery: Current Status and Future Direction. *Recent Res. Dev. Life Sci.* **2003**, *1* (2), 275–290.
- Zhu, J.; Mix, E.; Winblad, B. The Antidepressant and Anti-Inflammatory Effects of Rolipram in the Central Nervous System. *CNS Drug Rev.* **2001**, *7* (4), 387–398.
- Loughney, K.; Snyder, P. B.; Uher, L.; Rosman, G. J.; Ferguson, K.; Florio, V. A. Isolation and Characterization of PDE10A, A Novel Human 3'-5'-Cyclic Nucleotide Phosphodiesterase. *Gene* **1999**, *234*, 109–117.
- Soderling, S. H.; Bayuga, S. J.; Beavo, J. A. Isolation and Characterization of a Dual-Substrate Phosphodiesterase Gene Family: PDE10A. *Proc. Natl. Acad. Sci. U.S.A.* **1999**, *96*, 7071–7076.
- Fujishige, K.; Kotera, J.; Michibata, H.; Yuasa, K.; Takebayashi, S.; Okumura, K.; Omori, K. Cloning and Characterization of a Novel Human Phosphodiesterase that Hydrolyzes both cAMP and cGMP (PDE10A). *J. Biol. Chem.* **1999**, *274* (26), 18438–18445.
- Weston, M. C.; Holst, L. S.; Degerman, E.; Manganiello, V. C. cAMP/cGMP Dual-Specificity Phosphodiesterases. In *Handbook of Cell Signalling, Volume 2*; Dennis, R. A. B. a. E. A., Ed.; Academic Press: New York, 2003; Vol. 2, pp 441–446.
- Fujishige, K.; Kotera, J.; Omori, K. Striatum- and Testes-Specific Phosphodiesterase PDE10A. Isolation and Characterization of a Rat PDE10A. *Eur. J. Biochem.* **1999**, *266*, 1118–1127.
- Seeger, T. F.; Bartlett, B.; Coskran, T. M.; Culp, J. S.; James, L. C.; Krull, D. L.; Lanfear, J.; Ryan, A. M.; Schmidt, C. J.; Strick, C. A.; Varghese, A. H.; Williams, R. D.; Wylie, P. G.; Menniti, F. S. Immunohistochemical Localization of PDE10A in the Rat Brain. *Brain Res.* **2003**, *985*, 113–126.
- Siuciak, J. A.; Chapin, D. S.; Harms, J. F.; Lebel, L. A.; James, L. C.; McCarthy, S. A.; Chambers, L. K.; Shrikhande, A.; Wong, S. K.; Menniti, F. S.; Schmidt, C. J. Inhibition of the Striatum-Enrichment Phosphodiesterase PDE10A: A Novel Approach to the Treatment of Psychosis. *Neuropharmacology* **2006**, *51* (2), 386–396.
- Siuciak, J. A.; McCarthy, S. A.; Chapin, D. S.; Fujiwara, R. A.; James, L. C.; Williams, R. D.; Stock, J. L.; McNeish, J. D.; Strick, C. A.; Menniti, F. S.; Schmidt, C. J. Genetic Deletion of the Striatum-Enriched Phosphodiesterase PDE10A: A Novel Approach to the Treatment of Psychosis. *Neuropharmacology* **2006**, *51* (2), 374–385.
- Lebel, L. A.; Menniti, F. S.; Schmidt, C. J. Use of Selective PDE10 Inhibitors for the Treatment of Central Nervous System Disorders. *Eur. Pat. Appl.* 1 250 923 A2, Oct. 23, 2002.
- Allen, M. P.; Chappie, T. A.; Humphrey, J. M.; Liras, S. Tetrahydroisoquinoline Derivatives of Quinazoline and Isoquinoline. US20050182079 A1, Aug. 18, 2005.
- Pandit, J. Crystal Structure of 3',5'-Cyclic Nucleotide Phosphodiesterase (PDE10A) and Uses Thereof. US20050202550 A1, Sept. 15, 2005.
- Rocco, S. A.; Barbarini, J. E.; Rittner, R. Synthesis of Some 4-Anilinoquinazoline Derivatives. *Synthesis* **2004**, *3*, 429–435.
- Alexandre, F.; Berecibar, A.; Wrigglesworth, R.; Besson, T. Novel Series of 8H-Quinazolino[4,3-b]quinazoline-8-ones Via Two Nientowski Condensations. *Tetrahedron* **2003**, *59* (9), 1413–1419.
- Liu, X.; Narla, R. K.; Uckun, F. Organic Phenyl Arsenic Acid Compounds with Potent Antileukemic Activity. *Bioorg. Med. Chem. Lett.* **2003**, *13* (3), 581–583.
- Nagahara, T.; Yokoyama, Y.; Inamura, K.; Komoriya, S.; Yamaguchi, H.; Hara, T.; Iwanoto, M. Dibasic (Amindinoaryl)propanoic Acid Derivatives as Novel Blood Coagulation Factor Xa Inhibitors. *J. Med. Chem.* **1994**, *37*, 1200–1207.

JM060653B